Mechanism of charge transfer and its impacts on Fermi-level pinning for gas molecules adsorbed on monolayer WS2

Zhou, Changjie; Yang, Weihuang; Zhu, Huili

2015

Zhou, C., Yang, W., & Zhu, H. (2015). Mechanism of charge transfer and its impacts on Fermi-level pinning for gas molecules adsorbed on monolayer WS2. The journal of chemical physics, 142(21), 214704-.

https://hdl.handle.net/10356/106046

https://doi.org/10.1063/1.4922049

Mechanism of charge transfer and its impacts on Fermi-level pinning for gas molecules adsorbed on monolayer WS2

Changjie Zhou, Weihuang Yang, and Huili Zhu

Citation: The Journal of Chemical Physics **142**, 214704 (2015); doi: 10.1063/1.4922049
View online: http://dx.doi.org/10.1063/1.4922049
View Table of Contents: http://scitation.aip.org/content/aip/journal/jcp/142/21?ver=pdfcov
Published by the AIP Publishing

Mechanism of charge transfer and its impacts on Fermi-level pinning for gas molecules adsorbed on monolayer WS_2

Changjie Zhou,[1] Weihuang Yang,[2] and Huili Zhu[1,a)]
[1]*Department of Physics, School of Science, Jimei University, Xiamen 361021, People's Republic of China*
[2]*Division of Physics and Applied Physics, School of Physical and Mathematical Science, Nanyang Technological University, Singapore 637371*

(Received 1 March 2015; accepted 21 May 2015; published online 3 June 2015)

Density functional theory calculations were performed to assess changes in the geometric and electronic structures of monolayer WS_2 upon adsorption of various gas molecules (H_2, O_2, H_2O, NH_3, NO, NO_2, and CO). The most stable configuration of the adsorbed molecules, the adsorption energy, and the degree of charge transfer between adsorbate and substrate were determined. All evaluated molecules were physisorbed on monolayer WS_2 with a low degree of charge transfer and accept charge from the monolayer, except for NH_3, which is a charge donor. Band structure calculations showed that the valence and conduction bands of monolayer WS_2 are not significantly altered upon adsorption of H_2, H_2O, NH_3, and CO, whereas the lowest unoccupied molecular orbitals of O_2, NO, and NO_2 are pinned around the Fermi-level when these molecules are adsorbed on monolayer WS_2. The phenomenon of Fermi-level pinning was discussed in light of the traditional and orbital mixing charge transfer theories. The impacts of the charge transfer mechanism on Fermi-level pinning were confirmed for the gas molecules adsorbed on monolayer WS_2. The proposed mechanism governing Fermi-level pinning is applicable to the systems of adsorbates on recently developed two-dimensional materials, such as graphene and transition metal dichalcogenides. © *2015 AIP Publishing LLC.* [http://dx.doi.org/10.1063/1.4922049]

I. INTRODUCTION

Detection of gas molecules, especially toxic or hazardous gases, is an important issue in various fields, such as industry, agriculture, and public health.[1] Metal oxides are utilized in conventional chemical-sensing materials because of their high sensitivity and relatively low cost.[2–4] However, gas sensors based on metal oxides usually operate only at high temperatures in the range of 200–500 °C,[5] which leads to several attendant issues such as high power consumption and other safety problems. To resolve these issues, the development of highly sensitive gas sensors that can operate at room temperature has been actively pursued. In this respect, two-dimensional (2D) nanomaterials comprising graphene and transition-metal dichalcogenides (TMDCs) like MoS_2 and WS_2 have emerged as attractive prospectives.[6–13] The majority of gas sensors fabricated with these 2D nanomaterials are field-effect transistor (FET)-based devices.[13] The basic operating principle involves a reversible change of the electrical conductivity caused by the interaction between the 2D nanomaterials and the adsorbed gaseous species.

Gas sensors employing a graphene-based FET that is operative at room temperature have been successfully fabricated by Schedin *et al.* The sensing mechanism of the graphene-based sensor is derived from the doping behavior of the adsorbed molecules, that is donor or acceptor behavior, and is further due to the change in the resistivity of the base materials. Sensitivity to NH_3, CO, and H_2O at concentrations as low as 1 ppb has been demonstrated, and the ultimate sensitivity for an individual NO_2 molecule has even been achieved.[6] Similar to graphene, single and few-layer MoS_2 sheets are found to be sensitive detectors for NO, NO_2, NH_3, and triethylamine gas.[7–9,12] Most recently, the photoelectric properties of multilayer WS_2 nanoflakes, including their field-effect, photosensitivity, and gas sensitivity, have been empirically evaluated.[14] The photoresponsivity (R_λ) and external quantum efficiency (EQE) of WS_2 are significantly enhanced by inclusion of molecular NH_3. Maximum R_λ and EQE values of 884 A/W and 1.7×10^5% may, respectively, be achieved. In contrast, under O_2 or air atmosphere, the drain current of the device decreased compared to that under vacuum. Although the gas sensitivity and its effect on the photoresponse of the WS_2-FET sensor have been experimentally studied, the mechanism underlying the interaction of NH_3 and O_2 molecules with the WS_2 surface and the effect on the electronic properties remain undefined.

Moreover, the oxidizing or reducing characteristics of the adsorbed gas molecules, i.e., the charge transfer, depend largely on the interaction between the target gases and base materials and are not absolute. In the case of *n*-type metal oxides, the traditional reducing gases, such as CO, H_2O, H_2, NH_3, CH_4, and C_2H_5OH, donate electrons to the conduction band of the base material, whereas traditional oxidizing gases such as NO_x, Cl_2, O_2, and O_3 accept electrons.[5] In the case of *p*-type oxides, the reverse is the case.[5] However, H_2O molecules actually act as the oxidizing gas in the graphene- and MoS_2-based gas sensors,[6,15,16] in contrast to

a)Author to whom correspondence should be addressed. Electronic mail: hlzhu@jmu.edu.cn. Telephone: +86-592-6181891.

the case of metal oxides. For certain WS_2-based gas sensors, H_2O molecules have been found to act as the oxidizing gas upon adsorption on the layered WS_2,[14] whereas other studies show that H_2O is the reducing gas.[17] Therefore, exploration of the interaction between the adsorbed molecules and the WS_2 monolayer and assessment of the distinctive characteristics of the adsorbate/adsorbent system from the theoretical perspective are worthwhile pursuits.

Herein, we evaluate the adsorption of various gas molecules (H_2, O_2, H_2O, NH_3, NO, NO_2, and CO) on the WS_2 monolayer using first-principles calculations. The preferential binding configurations of these gas molecules are first obtained by calculating the adsorption energies. Charge transfer between the adsorbed molecules and the monolayer WS_2 is then theoretically quantified to determine the doping behavior of these adsorbates. Furthermore, Fermi-level pinning phenomena for these adsorption systems are discussed in light of the traditional and orbital mixing charge transfer theories. The impacts of the charge transfer mechanism on Fermi-level pinning are confirmed in the case of gas molecules adsorbed on monolayer WS_2.

It should be noted that at traditional metal-semiconductor junctions such as Al–Si junctions, there is usually a Schottky barrier with the Fermi-level pinned in the bandgap of the semiconductor at the interface region. The pinning positions vary within 0.2 eV, independent of the metal work function, crystallographic orientation, semiconductor doping concentration, interface impurities, etc.[18] The formation of interfacial gap states plays a key role in Fermi-level pinning in these situations. Distinct from the case encountered in metal-semiconductor contacts, the concept of Fermi-level pinning in the field of 2D nanomaterials discussed in this study indicates that the Fermi-level of the adsorbed gas/2D nanomaterial system is pinned around the lowest unoccupied molecular orbital (LUMO) or highest occupied molecular orbital (HOMO) of the adsorbed gas molecules. The phenomenon of Fermi-level pinning is associated with the energy level alignment and is further determined by the mechanism of charge transfer, i.e., the traditional and orbital mixing charge transfer theories. Thus, the effect of Fermi-level pinning should be considered when fabricating new optoelectronic and gas sensing devices based on these 2D nanomaterials.

II. CALCULATION DETAILS

We performed geometry relaxation, total energy, and electronic structure calculations using density functional theory (DFT), as implemented in the Vienna *ab initio* simulation package (VASP).[19,20] The most important parameter is the exchange-correlation functional. It is well known that the local density approximation (LDA) functional is more suitable than the generalized gradient approximation (GGA) functional for describing the interaction between molecules and graphene-like 2D materials.[16,21–23] GGA overestimates the separation between the 2D nanomaterials and molecules while LDA yields acceptable separations.[24,25] Therefore, the exchange-correlation interaction is treated herein by using LDA. The electron-ion interaction was approximated using the projector-augmented wave potential. The electron wavefunctions were expanded in plane waves with an energy cutoff of 500 eV. Supercells with 4×4 dimensions (16 W and 32 S atoms) were used to simulate individual monolayer WS_2. In order to avoid interlayer interactions, the distance between monolayers was set to more than 20 Å. The distance between two neighboring gas molecules was larger than 12 Å. The Brillouin-zone integrations were performed with a $5 \times 5 \times 1$ Monkhorst-Pack grid for k-point sampling.[26] Structural optimizations were carried out by relaxing all the atomic geometries using the conjugate gradient algorithm. The forces on all the atoms converged to within 0.02 eV/Å. The charge transfer between the WS_2 monolayer and the adsorbed gas molecules was also calculated using Bader analysis.[27]

III. RESULTS AND DISCUSSION

In the relaxed structure of pristine monolayer WS_2 (Fig. 1(a)), the planar projection shows a perfect hexagonal

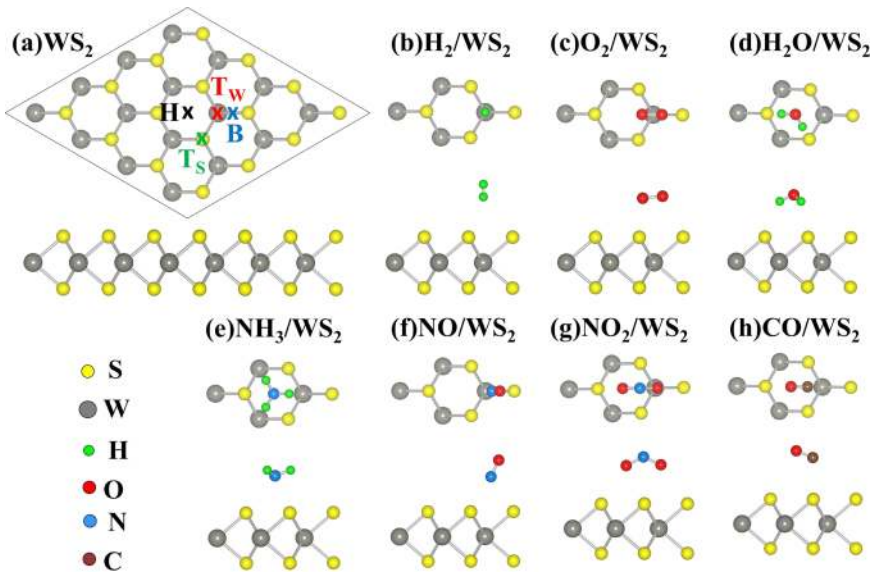

FIG. 1. Top and side views of (a) relaxed pristine monolayer WS_2, most favorable configurations for (b) H_2, (c) O_2, (d) H_2O, (e) NH_3, (f) NO, (g) NO_2, and (h) CO adsorbed on monolayer WS_2. Yellow and gray balls represent S and W atoms, whereas green, red, blue, and brown balls represent H, O, N, and C atoms, respectively. Four adsorption sites are labeled as "×," namely, the H site (on top of a hexagon), the Tw site (on top of a W atom), the Ts site (on top of a S atom), and the B site (on top of a W–S bond).

TABLE I. Calculated adsorption energy (E_a) and equilibrium height (h) for the adsorption of gas molecules (H_2, O_2, H_2O, NH_3, NO, NO_2, and CO) on monolayer WS_2.

	H site		Tw site		Ts site		B site	
Gas	h (Å)	E_a (meV)	h (Å)	E_a (meV)	h (Å)	E_a (meV)	h (Å)	E_a (meV)
H_2	2.86	−68	2.86	−75	2.87	−37	...	...
O_2	2.62	−184	2.49	−213	3.09	−119	...	...
H_2O	2.63	−229	2.68	−218	3.14	−108	...	...
NH_3	2.49	−216	2.76	−201	3.25	−62	...	...
NO	2.77	−129	2.77	−206	3.47	−99	2.76	−215
NO_2	2.68	−412	...	...	2.68	−354	2.74	−333
CO	2.90	−127	2.90	−111	2.95	−31	2.90	−75

lattice of S atoms, with interleaved W atoms that are coordinated by S atoms in a trigonal prismatic arrangement. The optimized lattice constant of monolayer WS_2 determined from the present calculation is about 3.13 Å, which agrees well with the experimental value of 3.15 Å.[28] Since monolayer WS_2 belongs to the $P\bar{6}m2$ space group, four adsorption sites were considered to determine the favorable adsorption configuration, including the center of a hexagon (H), the top of a W atom (Tw), the top of a S atom (Ts), and the center of a W–S bond (B), as indicated in Fig. 1(a). Moreover, two orientations of the NH_3 molecule were investigated for each anchoring position, one with the H atoms pointing away from the monolayer WS_2 surface and the other with the H atoms pointing towards the surface. For other gas molecules, such as H_2, O_2, H_2O, NO, NO_2, and CO, three orientations with respect to the WS_2 surface were examined. Taking H_2O as an example, the three involved orientations are the H–O bonds pointing up, down, or parallel to the surface. The adsorption energy, E_a, is calculated as $E_a = [E_{mol/WS_2} - E_{WS_2}]/N - E_{mol}$, where E_{mol/WS_2}, E_{WS_2}, and E_{mol} are the total energies of the surface with N adsorbates, the clean surface, and an isolated molecule, respectively.

The calculated E_a and equilibrium height (h) obtained at different anchoring positions are listed in Table I. Negative adsorption energy means that the adsorption process is exothermic and energetically favored (stable). The equilibrium height is the space between the upper S-layer and the center of mass of the gas molecule. The structural relaxations show that the H_2, O_2, NH_3, and H_2O molecules fail to have a stable configuration at the B site, while NO_2 fails to localize at the Tw site because these molecules tend to migrate to other sites during the relaxations. From the results presented in Table I, it is apparent that for H_2 and O_2, the Tw site is the most favorable site with adsorption energies of −75 and −213 meV, respectively. Correspondingly, H_2 adsorbed on the Tw site has the minimum equilibrium height of 2.86 Å with respect to monolayer WS_2, which is about 1.47 Å longer than the total lengths of the S and H covalent radii. O_2 on the Tw site has the minimum equilibrium height of 2.49 Å, which is about 1.24 Å longer than the total lengths of the S and O covalent radii. H_2O, NH_3, NO_2, and CO are preferably adsorbed at the H site with adsorption energies of −229, −216, −412, and −127 meV, respectively. The minimum equilibrium heights for the four systems of adsorbed gas are about 1 Å longer than the total lengths of the covalent radii of the S atom and the lowest atom of the adsorbed molecules. In contrast, NO is preferably located at the B site with the adsorption energy of −215 meV. NO adsorbed on the B site has the minimum equilibrium height of 2.76 Å, which is about 0.99 Å longer than the total lengths of the S and N covalent radii. The low adsorption energy and large separation height indicate that all gas molecules examined in this study are physisorbed on the WS_2 surface. On the basis of the negative and low adsorption energies, monolayer WS_2 should be applicable for detection of all proposed gas molecules since the adsorption-desorption equilibrium of the adsorbed gas molecules on monolayer WS_2 can be easily established.

The top and side views of the most favorable configurations for H_2, O_2, H_2O, NH_3, NO, NO_2, and CO adsorbed on monolayer WS_2 are shown in Figs. 1(b)-1(h), respectively. The configurations of the H_2 and O_2 molecules show that H_2 and O_2 are both adsorbed directly on top of the Tw site. H_2 has an axis perpendicular to the WS_2 surface, while O_2 is nearly parallel to the WS_2 surface with its center of mass on top of the Tw site. The configurations of the H_2O, NH_3, NO_2, and CO molecules show that these four molecules are adsorbed on top of the hexagon formed by the W and S atoms. The O atom of the H_2O molecule occupies the center of the hexagon. The O–H bonds point towards the S atoms and adopt a tilted orientation with the two H atoms pointing towards the WS_2 surface. In contrast, the NH_3 molecule adopts a configuration in which the N atom occupies the center of the hexagon. The N–H bonds point towards the W atoms and adopt a tilted orientation with all the H atoms pointing away from the WS_2 surface. In contrast with the configurations of H_2O and NH_3, the NO_2 and CO molecules stretch across the hexagon along the plane from the center of the hexagon to the W atom. NO_2 is bonded in a configuration whereby the O atoms are positioned close to the WS_2 surface, whereas CO is bonded with the C atom positioned close to the WS_2 surface. In contrast to the other gas molecules, NO is preferentially localized at the B site. N–O is bonded parallel to W–S and adopts a tilted orientation with the N atom pointed toward the surface. The different adsorption orientations of these gas molecules on the WS_2 surface exert a significant influence on the electronic properties of the adsorption systems, as discussed below. The ensuing results for these gas molecules were obtained based on the most favorable configurations presented above.

To gain insight into the charge redistribution in real space and the interaction between the adsorbates and the underlying

WS_2 monolayer, the differential charge densities (DCD) of the adsorbed configurations were calculated by using the formula: $\Delta\rho_{mol/WS_2} = \rho_{mol/WS_2} - \rho_{mol} - \rho_{WS_2}$, where ρ_{mol/WS_2}, ρ_{WS_2}, and ρ_{mol} are the charge density of the molecule-adsorbed system, the monolayer WS_2, and an isolated molecule, respectively. The values of ρ_{WS_2} and ρ_{mol} were obtained by using the optimized structures of the molecules adsorbed on monolayer WS_2. The calculated side views of the DCD isosurface are shown in Fig. 2. The region of electron accumulation (depletion) on the DCD isosurface is indicated by yellow (blue). The WS_2 monolayer and the gas molecules are both considerably polarized due to the charge redistribution in real space. Consequently, electrostatic interactions play a role in the attractive interaction. Based on careful comparison of the DCD isosurfaces shown in Fig. 2, polarization is found to be stronger in the case of O_2, H_2O, NH_3, NO, and NO_2 than in the case of H_2 and CO. The stronger polarization is expected to give rise to larger interaction energy, which is consistent with the trends in the adsorption energies observed above. The energies of adsorption of O_2, H_2O, NH_3, NO, and NO_2 on the WS_2 surface were −213, −229, −216, −215, and −412 meV, respectively (Table I); these values are larger than those of H_2 (−75 meV) and CO (−127 meV).

Charge transfer in the adsorption systems of these gas molecules adsorbed on monolayer WS_2 was evaluated based on charge analysis using the Bader scheme, which provides an intuitive way of separating the charge related to each atom using first-principles calculations. Bader analysis (Fig. 2) shows that NH_3 contributes 0.061 e to the WS_2 monolayer and is an electron donor, whereas the other gas molecules are charge acceptors that receive 0.002–0.178 e from the WS_2 monolayer. The charge transfer values are similar to those presented in previous reports for the adsorption of gas molecules on graphene[15] and monolayer MoS_2.[16] It may be difficult to detect H_2, CO, and NO on the basis of charge transfer given that the charge transfer contributions of these molecules are quite small. However, O_2, H_2O, NO_2, and NH_3 can be physically adsorbed on monolayer WS_2 with moderate adsorption energies, accompanying non-negligible charge transfer. Therefore, monolayer WS_2 may be a promising candidate as a sensor for O_2, H_2O, NO_2, and NH_3.

The mechanism by which the WS_2-FET gas sensor[14] detects O_2 and NH_3 can thus be understood as follows. Because layered WS_2 has *n*-type conductivity in the experiment,[14] some electrons are present in the channel of the WS_2-FET gas sensor. When exposed to an NH_3 atmosphere, the *n*-type WS_2 channel obtains more electrons from the adsorbed gas molecules, thereby enhancing the total conduction electron density and resulting in a significant increase of R_λ and EQE. In contrast, O_2 molecules trap electrons from the *n*-type WS_2 channel and quench the source-drain current of the WS_2-FET gas sensor.

For comparison with real WS_2-FET devices and to evaluate the different responses under NH_3 and O_2 atmosphere, the differential saturation source-drain current (ΔI_{Dsat}) at zero gate voltage was estimated as $\Delta I_{Dsat} = q\Delta n_{2D}\frac{W\mu}{2L}(-V_T)$, where W is the channel width (15 μm), L is the channel length (20 μm), and Δn_{2D} is the 2D carrier concentration increment; μ and V_T are the field-effect carrier mobility (12 cm^2/Vs)[14,29] and threshold voltage (−3.5 V)[14] of WS_2, respectively. The 2D electron density increased by 3.8×10^{12} cm^{-2} after adsorption of one NH_3 molecule on the 4×4 WS_2 supercell. Thus, the saturation source-drain current, I_{Dsat}, increased by 9.6×10^{-6} A as compared to that under vacuum, which is consistent with the experimentally observed significant increase of the dark drain current (V_{DS} = 1 V) by $\sim 6.9 \times 10^{-7}$ A in response to NH_3.[14] When one O_2 molecule was adsorbed, the decrease in the 2D electron density was quantified as

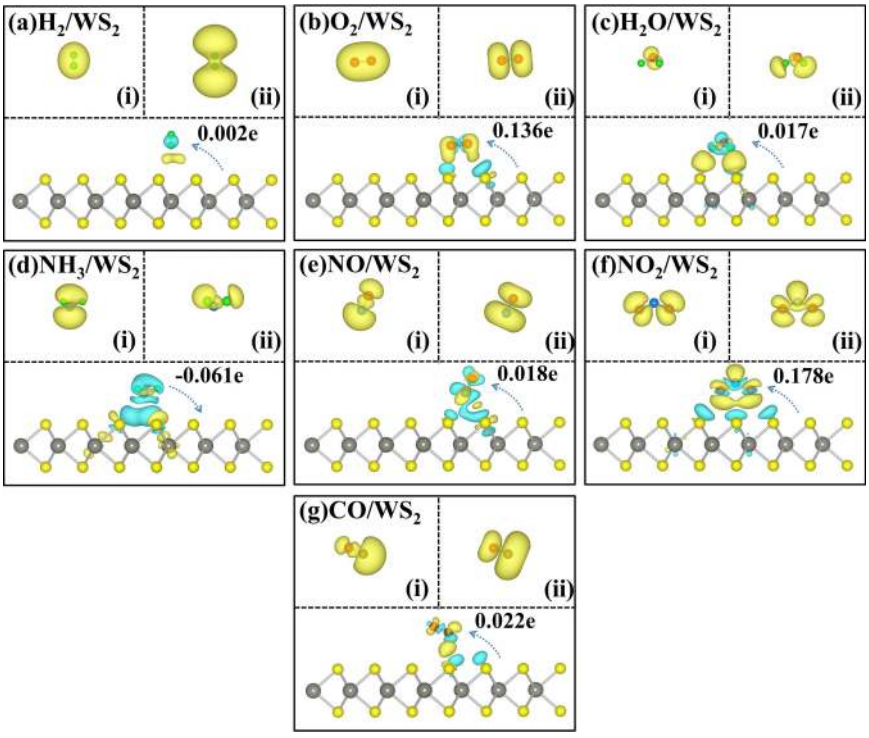

FIG. 2. Side views of the DCD for (a) H_2, (b) O_2, (c) H_2O, (d) NH_3, (e) NO, (f) NO_2, and (g) CO interacting with monolayer WS_2. The isosurface for O_2, H_2O, NH_3, NO, and NO_2 is taken as 6.0×10^{-4} e/Å^3, while that for H_2 and CO is taken as 3.0×10^{-4} e/Å^3. The electron accumulation (depletion) region on the DCD isosurface is indicated by yellow (blue). The direction (indicated by an arrow) and value of the charge transfer are shown. Insets (i) and (ii) in (a)-(g), respectively, show the HOMO and LUMO of a single gas molecule.

8.4×10^{12} cm^{-2} and I_{Dsat} decreased by 2.1×10^{-5} A, consistent with the significant experimentally observed decrease of the dark drain current (V_{DS} = 1 V) to ~1.0×10^{-8} A in response to O_2. Therefore, the theoretical data for adsorption of NH_3 and O_2 on monolayer WS_2 obtained herein are consistent with the most recent experimental results, and the electrical sensitivities to gas adsorption make WS_2 a promising gas sensor for a wide range of applications.

To further identify the influence of the adsorption of various gas molecules on the electronic properties of monolayer WS_2, the energy band structures of the adsorbate-adsorbent systems of gas molecules and WS_2 were calculated, as shown in Fig. 3. For comparison, the energy band structure of pristine monolayer WS_2 is also presented in Fig. 3(a). The direct bandgap of pristine monolayer WS_2 between the top of the valance band and the bottom of the conduction band at the K-point, calculated using LDA, is about 1.984 eV, which agrees well with the experimental result of about 2.0 eV.[30,31] The bandgap for the valence and conduction bands of monolayer WS_2 remain largely unaltered when H_2, H_2O, NH_3, and CO are adsorbed, except for a slight reduction of the bandgap in the case of NH_3 adsorption, as shown in Figs. 3(b), 3(d), 3(e), and 3(h), respectively. In the case of adsorption of NH_3, the bandgap energy is reduced to 1.967 eV, which is a 0.017 eV reduction compared to that of pristine monolayer WS_2. The bandgap reduction is attributed to slight orbital hybridization between NH_3 and the underlying WS_2 in the valence band, which further splits the valence band and reduces the bandgap of monolayer WS_2, as shown in Fig. 3(d). Moreover, no impurity states were formed in the bandgap of monolayer WS_2 during adsorption of the four aforementioned gases. In contrast, some flat impurity states are clearly observed in the bandgap of the host monolayer when O_2, NO, and NO_2 are adsorbed. These flat impurity states induced by introduction of O_2, NO, and NO_2 are mostly distributed near the Fermi-level. That is, the impurity states of these adsorbates are pinned around the Fermi-level upon adsorption of the gases on monolayer WS_2. The phenomenon of Fermi-level pinning in the case of gas molecules (H_2, O_2, H_2O, NH_3, NO, NO_2, and CO) adsorbed on two-dimensional materials has not previously been systematically evaluated. Notably, although adsorption of O_2, NO, and NO_2 induced formation of flat impurity states in the bandgap of monolayer WS_2, it should be emphasized that these impurity states in the projected energy band structures, as shown in Figs. 3(c), 3(f), and 3(g), have almost no influence on the bandgap energy of pristine WS_2 due to the weak physisorption interaction. Moreover, these impurity states are all localized around the adsorbed gas molecules because there is no hybridization between these impurity states and the base monolayer WS_2.

To elucidate the origin of the flat impurity states in the case of O_2, NO, and NO_2 adsorbed on monolayer WS_2 as shown in Fig. 3, the partial charge densities of the adsorption systems in the energy window (±0.1 eV) around the flat

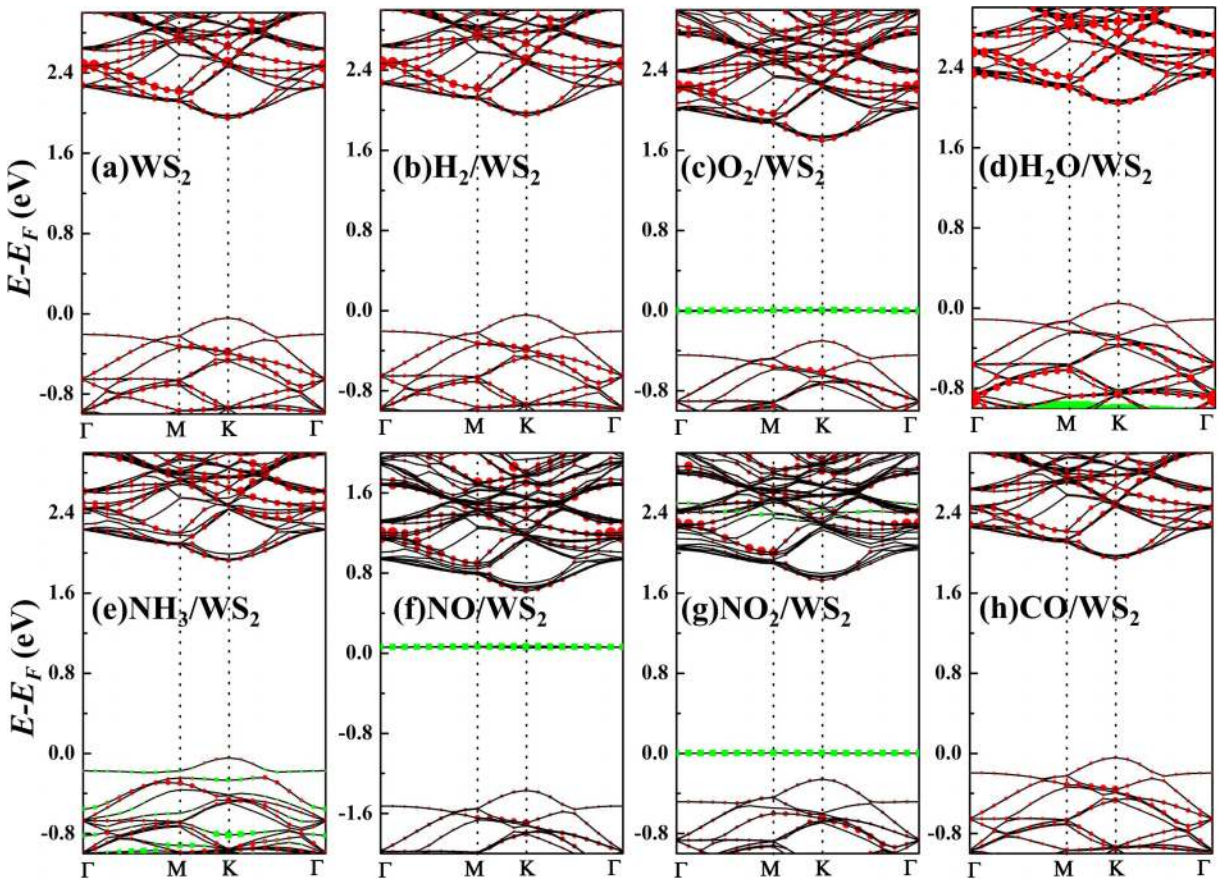

FIG. 3. (a) Band structure of pristine monolayer WS_2. (b)-(h) Band structures of H_2, O_2, H_2O, NH_3, NO, NO_2, and CO adsorbed on monolayer WS_2, respectively. The black curves in (a)-(h) are the overall band structures. The spherical red dots represent the projection of the W atom, while the green square dots represent the projection of the adsorbed gas molecules.

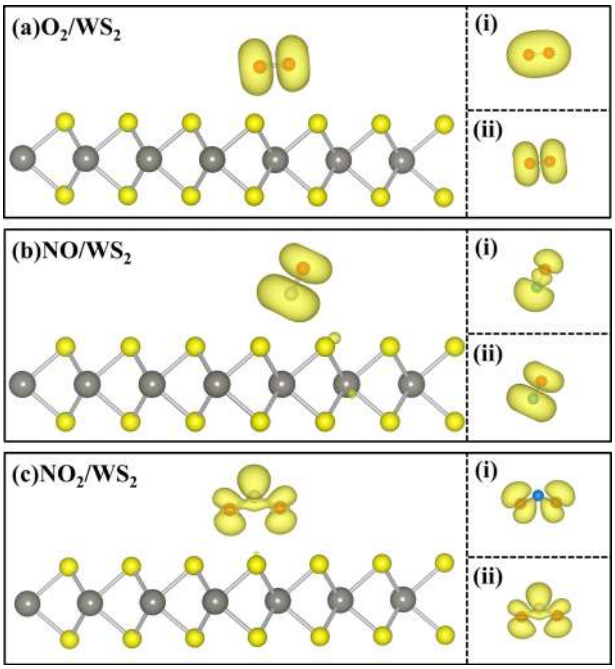

FIG. 4. Side views of the 0.005 e/Å^3 partial charge density isosurface of (a) O_2, (b) NO, and (c) NO_2 adsorbed on monolayer WS_2, calculated in an energy window (±0.1 eV) around the flat impurity states as shown in Fig. 3. Insets (i) and (ii) in (a)-(c), respectively, show the HOMO and LUMO of a single gas molecule.

impurity states were simulated, as shown in Fig. 4. For comparison, the LUMO and HOMO of the single gas molecule are shown in insets (i) and (ii), respectively. The partial charge densities originating from the flat impurity states exhibit the typical features of the LUMO of the adsorbed gas molecules. Therefore, the flat impurity states pinned to the Fermi-level are associated with the molecular LUMO of the gas molecules. In other words, the LUMO of O_2, NO, and NO_2 is pinned around the Fermi-level upon adsorption on monolayer WS_2. However, the other molecules H_2, H_2O, NH_3, and CO do not exhibit Fermi-level pinning.

In order to elucidate the impact of charge transfer on the Fermi-level pinning, the charge transfer mechanism of gas molecules adsorbed on monolayer WS_2 was investigated. The traditional charge transfer theory holds that if the molecular LUMO is lower than the WS_2 Fermi-level, the electron density drifts from WS_2 to the adsorbate; similarly, if the molecular HOMO is higher than the WS_2 Fermi-level, electron density is transferred from the adsorbate to WS_2. However, if the WS_2 Fermi-level lies between the HOMO and LUMO of the adsorbed molecule, no electron density is transferred between the adsorbate and the underlying WS_2. Figure 5(a) presents a schematic summary of the energies of the molecular HOMO, LUMO, and the Fermi-level of the adsorbate-adsorbent systems and a comparison of these energies with the Fermi-level of monolayer WS_2. The molecular LUMO of O_2, NO, and NO_2 is found to be lower than the WS_2 Fermi-level; therefore, electron density drifts from WS_2 to the adsorbed molecules, which is consistent with the aforementioned results of the Bader analysis. However, for H_2, H_2O, NH_3, and CO, the WS_2 Fermi-level lies between the molecular HOMO and LUMO of these adsorbed molecules. Based on the traditional charge transfer theory, there is no charge transfer between the gas molecule and the underlying WS_2, which is apparently contrary to the results of the Bader analysis. Therefore, in the case of H_2, H_2O, NH_3, and CO adsorbed on monolayer WS_2, the charge transfer mechanism cannot be accounted for based on the traditional theory, as described above.

Recently, research by Leenaerts[15] demonstrated that the mechanism of charge transfer between an adsorbate and substrate is also partially determined by mixing of the molecular HOMO and LUMO with the substrate orbitals. To depict the charge transfer mechanism, the HOMO and LUMO of the single gas molecule are simulated and shown in the insets of Fig. 2. The HOMO and LUMO of a single gas molecule are found to show different distributions. When the most favorable configurations of the molecules adsorbed on monolayer WS_2 are considered, as shown in Fig. 1, the interaction between the molecular HOMO and the underlying WS_2 orbitals is expected to be different from that of the molecular LUMO. Thus, orbital mixing would have a significant effect on the charge transfer for these adsorbed systems. Taking H_2O as an example, the HOMO is completely localized on the O atom. The LUMO is localized primarily on the H atoms and may be slightly delocalized unto the O atom. Considering the most favorable

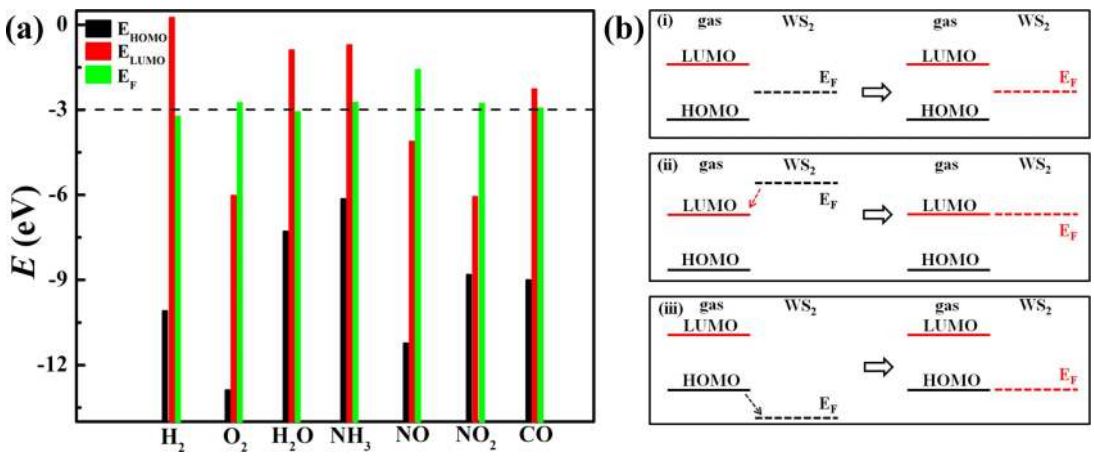

FIG. 5. (a) Molecular HOMO and LUMO levels and Fermi-levels of the adsorbed systems. The dashed line indicates the Fermi-level of monolayer WS_2 with the vacuum level shifted to zero. (b) Schematic plots of the relationship between charge transfer and Fermi-level pinning for gas molecules adsorbed on monolayer WS_2.

configuration of adsorbed H_2O (Fig. 1(d)) in which the H atoms point towards the monolayer, interaction with the WS_2 surface occurs primarily via the LUMO and the HOMO will provide a minor interaction due to the tilted configuration. Based on the 6.0×10^{-4} e/Å^3 DCD isosurface of adsorbed H_2O shown in Fig. 2(d), the increased DCD distribution is located on the H and O atoms, similar to the LUMO of isolated H_2O. Furthermore, a smaller decrease of the DCD distribution is also observed on the O atom, similar to that observed for the HOMO of isolated H_2O. Therefore, a large amount of charge is transferred from WS_2 to the LUMO of H_2O, while a smaller amount of charge is transferred from the HOMO of H_2O to monolayer WS_2. As a consequence, a small amount of charge will be transferred from WS_2 to H_2O. The acceptor character of H_2O adsorbed on WS_2 is consistent with the experimental results.[14] Therefore, charge transfer between the molecules (H_2, H_2O, NH_3, and CO) and substrate is governed by the orbital mixing theory rather than the traditional theory.

Based on the traditional and orbital mixing charge transfer theories discussed above, the mechanism of Fermi-level pinning can be distinguished for various gas molecules adsorbed on monolayer WS_2, as shown in Fig. 5(b). Case (i): if the WS_2 Fermi-level lies between the molecular HOMO and LUMO, then charge transfer is mainly governed by the orbital mixing theory and no Fermi-level pinning is observed as in the case of H_2, H_2O, NH_3, and CO upon adsorption on monolayer WS_2. Case (ii): if the molecular LUMO is lower than the WS_2 Fermi-level, electron density drifts from WS_2 to the adsorbed molecule and the molecular LUMO is pinned around the Fermi-level upon adsorption on WS_2 as in the cases of O_2, NO, and NO_2 adsorbed on monolayer WS_2. Case (iii): if the molecular HOMO is higher than the WS_2 Fermi-level, then electron density is transferred from the adsorbed molecule to WS_2 and the molecular HOMO is pinned around the Fermi-level upon adsorption on WS_2. Thus, Fermi-level pinning is evidently governed by the charge transfer mechanism. In fact, in one recent theoretical study,[16] Fermi-level pinning was observed for gas molecules adsorbed on monolayer MoS_2, where the adsorption of NO, NO_2, and O_2 also induced the generation of flat impurity states around the Fermi-level of the adsorbed system. The phenomenon of Fermi-level pinning has also been observed for a monolayer of electro-active conjugated molecules on graphene.[32] Therefore, the proposed mechanism governing the Fermi-level pinning is also applicable to the system of adsorbates on recently developed two-dimensional materials, such as graphene and TMDCs.

IV. CONCLUSIONS

In summary, the structural and electronic properties of monolayer WS_2 upon adsorption of various gas molecules (H_2, O_2, H_2O, NH_3, NO, NO_2, and CO) were evaluated. The exact orientations and the favorable binding sites on the monolayer WS_2 surface were determined by calculating the adsorption energy. Bader analysis demonstrates that all physisorbed gas molecules act as charge acceptors, except for NH_3 which is a charge donor. In contrast with H_2, CO, and NO for which the degree of charge transfer is low, O_2, H_2O, NO_2, and NH_3 can be physically adsorbed on the monolayer WS_2 with moderate adsorption energies, accompanying a moderate degree of charge transfer. Therefore, monolayer WS_2 may be a promising candidate as a sensor for O_2, H_2O, NO_2, and NH_3. These theoretical results for adsorption of NH_3 and O_2 on monolayer WS_2 are consistent with the most recent experimental data and suggest that WS_2 is a prospective material for gas sensing applications.

Furthermore, band structure calculations show that the valence and conduction bands of monolayer WS_2 are not significantly altered upon adsorption of H_2, H_2O, NH_3, and CO, whereas the molecular LUMO of O_2, NO, and NO_2 is pinned around the Fermi-level upon adsorption on the WS_2 surface. The charge transfer mechanism and its impacts on Fermi-level pinning were further examined based on the traditional and orbital mixing charge transfer theories. The mechanism of Fermi-level pinning is proposed to be governed by the charge transfer mechanism; this mechanism is also applicable for the system of adsorbates on recently developed two-dimensional materials.

ACKNOWLEDGMENTS

The authors gratefully acknowledge the financial support from the Natural Science Foundation of Fujian Province of China (Grant Nos. 2011J05006 and 2009J05149), the financial support from Department of Education of Fujian Province (Grant No. JA09146), Huang Hui Zhen Foundation of Jimei University (Grant No. ZC2010014), and the Scientific Research Foundation of Jimei University (Grant Nos. ZQ2011008 and ZQ2009004).

[1] J. Kong, N. R. Franklin, C. W. Zhou, M. G. Chapline, S. Peng, K. J. Cho, and H. J. Dai, Science **287**, 622 (2000).
[2] G. F. Fine, L. M. Cavanagh, A. Afonja, and R. Binions, Sensors **10**, 5469 (2010).
[3] S. J. Pearton, F. Ren, Y. L. Wang, B. H. Chu, K. H. Chen, C. Y. Chang, W. Lim, J. S. Lin, and D. P. Norton, Prog. Mater. Sci. **55**, 1 (2010).
[4] J. Huang and Q. Wan, Sensors **9**, 9903 (2009).
[5] G. Korotcenkov, Mater. Sci. Eng., B **139**, 1 (2007).
[6] F. Schedin, A. K. Geim, S. V. Morozov, E. W. Hill, P. Blake, M. I. Katsnelson, and K. S. Novoselov, Nat. Mater. **6**, 652 (2007).
[7] D. J. Late, Y. K. Huang, B. Liu, J. Acharya, S. N. Shirodkar, J. J. Luo, A. M. Yan, D. Charles, U. V. Waghmare, V. P. Dravid, and C. N. R. Rao, ACS Nano **7**, 4879 (2013).
[8] H. Li, Z. Y. Yin, Q. Y. He, H. Li, X. Huang, G. Lu, D. W. H. Fam, A. I. Y. Tok, Q. Zhang, and H. Zhang, Small **8**, 63 (2012).
[9] Q. Y. He, Z. Y. Zeng, Z. Y. Yin, H. Li, S. X. Wu, X. Huang, and H. Zhang, Small **8**, 2994 (2012).
[10] K. Lee, R. Gatensby, N. McEvoy, T. Hallam, and G. S. Duesberg, Adv. Mater. **25**, 6699 (2013).
[11] Y. G. Yao, L. Tolentino, Z. Z. Yang, X. J. Song, W. Zhang, Y. S. Chen, and C. P. Wong, Adv. Funct. Mater. **23**, 3577 (2013).
[12] F. K. Perkins, A. L. Friedman, E. Cobas, P. M. Campbell, G. G. Jernigan, and B. T. Jonker, Nano Lett. **13**, 668 (2013).
[13] B. Cho, M. G. Hahm, M. Choi, J. Yoon, A. R. Kim, Y. J. Lee, S. G. Park, J. D. Kwon, C. S. Kim, M. Song, Y. Jeong, K. S. Nam, S. Lee, T. J. Yoo, C. G. Kang, B. H. Lee, H. C. Ko, P. M. Ajayan, and D. H. Kim, Sci. Rep. **5**, 8052 (2015).
[14] N. J. Huo, S. X. Yang, Z. M. Wei, S. S. Li, J. B. Xia, and J. B. Li, Sci. Rep. **4**, 5209 (2014).
[15] O. Leenaerts, B. Partoens, and F. M. Peeters, Phys. Rev. B **77**, 125416 (2008).
[16] Q. Yue, Z. Z. Shao, S. L. Chang, and J. B. Li, Nanoscale Res. Lett. **8**, 425 (2013).
[17] M. Donarelli, S. Prezioso, F. Perrozzi, F. Bisti, M. Nardone, L. Giancaterini, C. Cantalini, and L. Ottaviano, Sens. Actuators, B **207**, 602 (2015).

[18]C. Gong, L. Colombo, R. M. Wallace, and K. Cho, Nano Lett. **14**, 1714 (2014).
[19]G. Kresse and J. Hafner, Phys. Rev. B **47**, 558 (1993).
[20]G. Kresse and J. Furthmüller, Phys. Rev. B **54**, 11169 (1996).
[21]J. W. Li, N. V. Medhekar, and V. B. Shenoy, J. Phys. Chem. C **117**, 15842 (2013).
[22]J. Y. Xi, T. Q. Zhao, D. Wang, and Z. G. Shuai, J. Phys. Chem. Lett. **5**, 285 (2014).
[23]H. Terrones, F. Lopez-Urias, and M. Terrones, Sci. Rep. **3**, 1549 (2013).
[24]A. Rochefort and D. Wuest, Langmuir **25**, 210 (2009).
[25]M. M. Li, J. Zhang, F. J. Li, F. X. Zhu, M. Zhang, and X. F. Zhao, Phys. Status Solidi C **6**, S90 (2009).
[26]H. J. Monkhorst and J. D. Pack, Phys. Rev. B **13**, 5188 (1976).
[27]G. Henkelman, A. Arnaldsson, and H. Jonsson, Comput. Mater. Sci. **36**, 354 (2006).
[28]W. J. Schutte, J. L. Deboer, and F. Jellinek, J. Solid State Chem. **70**, 207 (1987).
[29]B. Radisavljevic, A. Radenovic, J. Brivio, V. Giacometti, and A. Kis, Nat. Nanotechnol. **6**, 147 (2011).
[30]Y. D. Ma, Y. Dai, M. Guo, C. W. Niu, J. B. Lu, and B. B. Huang, Phys. Chem. Chem. Phys. **13**, 15546 (2011).
[31]G. L. Frey, R. Tenne, M. J. Matthews, M. S. Dresselhaus, and G. Dresselhaus, J. Mater. Res. **13**, 2412 (1998).
[32]L. P. Chen, L. J. Wang, Z. G. Shuai, and D. Beljonne, J. Phys. Chem. Lett. **13**, 2158 (2013).